Patricia

Guillermo

" In memoriam"

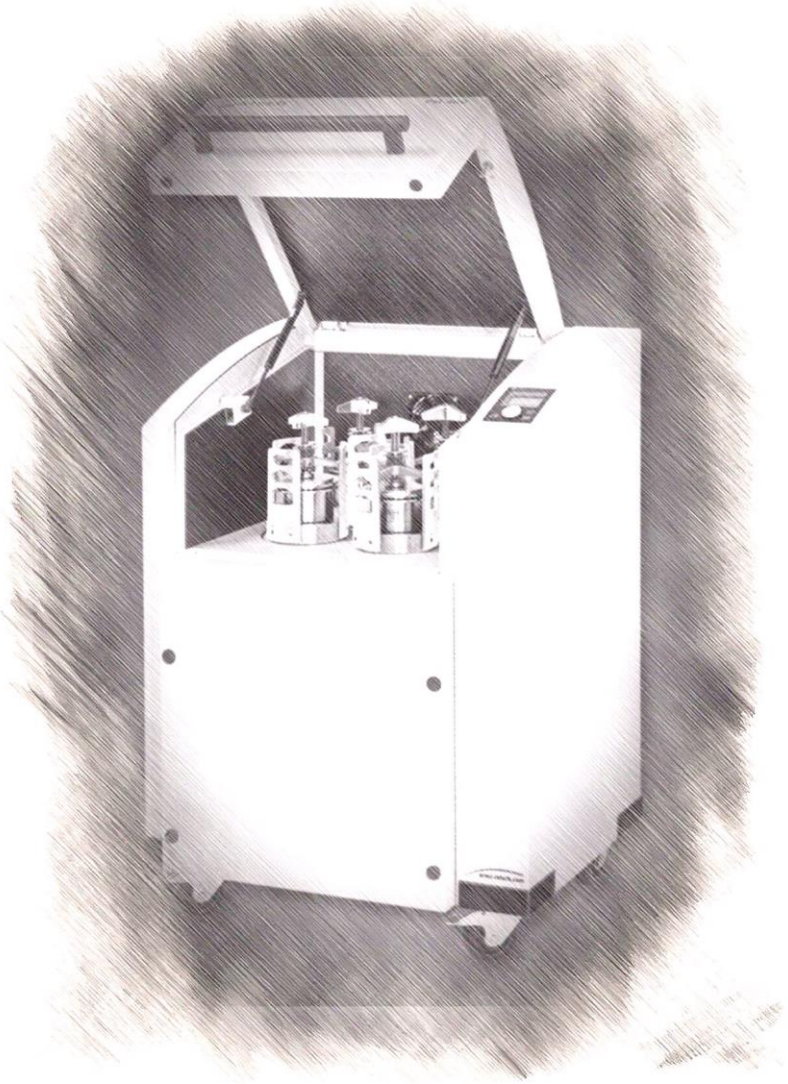

Aleado Mecánico

SQUID

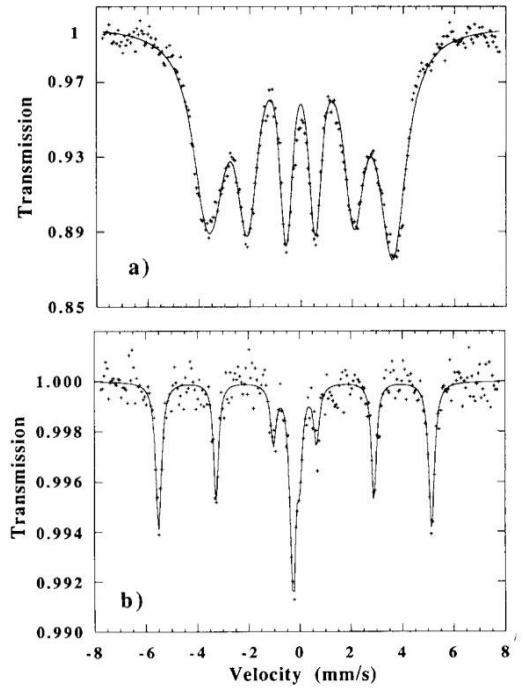

Fig. 3. Room temperature Mössbauer spectra for (a) as-milled and (b) annealed samples. The spectrum in (a) shows a broad distribution of hyperfine fields centered at 21 T and an isomer shift of $+0.1$ mms^{-1} relative to α-Fe at room temperature. The shoulder in the central peak in spectrum (b) shows the existence of a number of paramagnetic Fe atoms in the neighborhood of Cu atoms (see the text).

Mossbauer

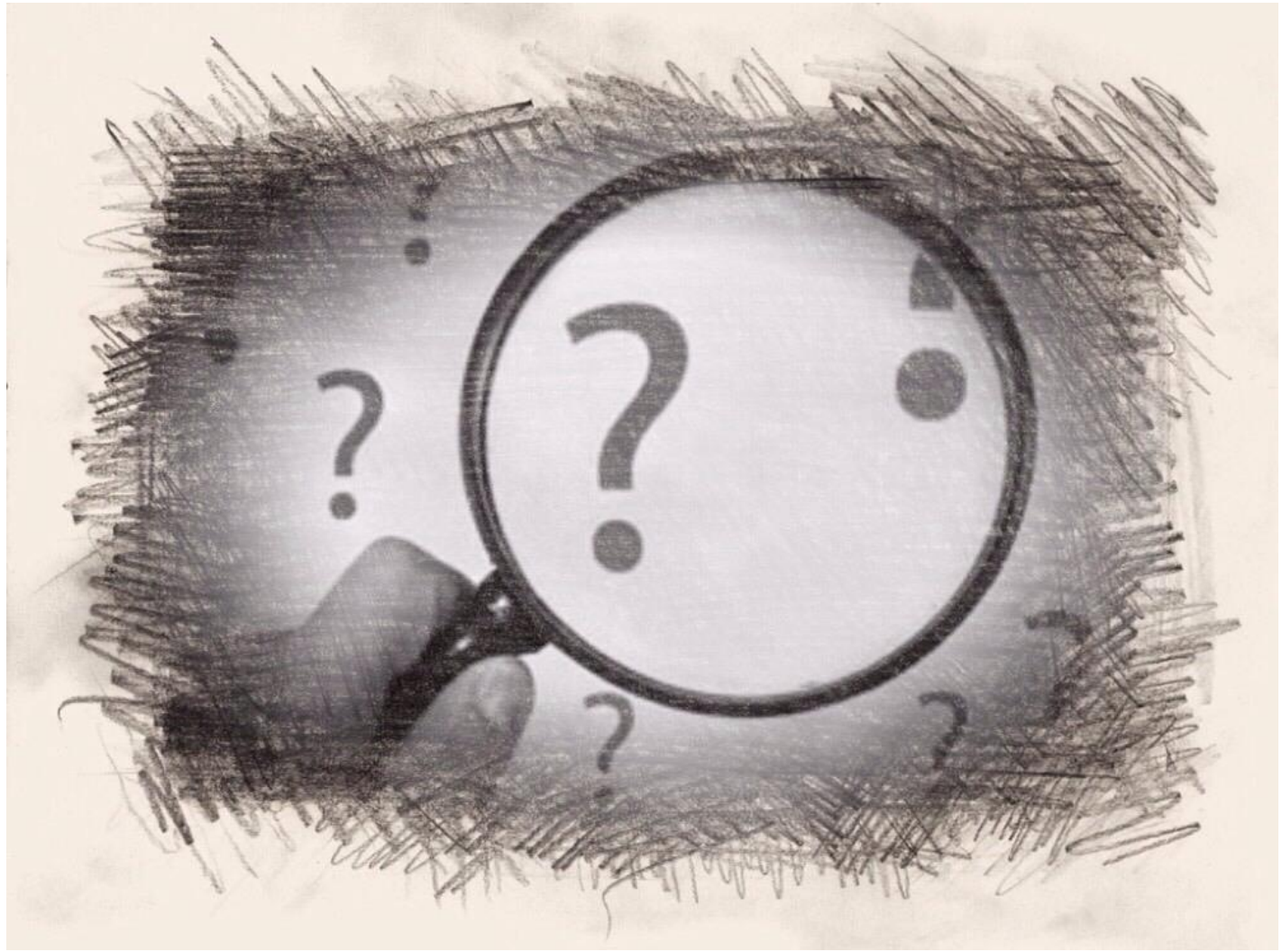

Ferromagnetismo

¿ Dónde estás?

+

Fe *Cu*

Catálogo Cisne **UCM - AECID**

Autor	Crespo del Arco, Patricia
Título	**Propiedades magnéticas de aleaciones nanocristalinas de Fe-Cu. / Patricia Crespo del Arco ; [director] Antonio Hernando Grande**
Publicación	1993
Colección	Universidad Complutense de Madrid. Facultad de Ciencias Físicas. Departamento de Física de Materiales. Tesis inéditas

Journal of Magnetism and Magnetic Materials 124 (1993) 5–8
North-Holland

journal of magnetism and magnetic materials

Letter to the Editor

Magnetic properties of mechanically alloyed Fe–Cu

A. Hernando and P. Crespo
Instituto de Magnetismo Aplicado, UCM-RENFE, P.O. Box 155, Las Rozas, 28230 Madrid, Spain

J.M. Barandiaran
Universidad del País Vasco, 48080 Bilbao, Spain

A. García Escorial
CENIM-CSIC, Avda. G. Del Amo 8, 28040 Madrid, Spain

R. Yavari
LTPCM, Institute National Polytechnique de Grenoble, St. Martin d'Hères 38402, France

Received 25 September 1992; in revised form 22 February 1993

Magnetic properties of equiatomic FeCu alloys, obtained by mechanical alloying, were measured in a temperature range between 5 and 300K. The as-milled sample consists of a metastable fcc FeCu phase with a temperature dependence of magnetization which follows a $T^{3/2}$ law. This metastable phase decomposes into Cu and Fe phases with annealing. After annealing at 820K, the magnetization value at low temperature is 30% smaller than the unannealed state. The Mössbauer spectrum obtained at room temperature shows a paramagnetic Fe phase with a relative resonant area of 30%. These results suggest that after this annealing process 30% of the iron is not in the ferromagnetic α phase but in a non-magnetic state (with vanishing atomic magnetic moment) or probably forming an antiferromagnetic γ-Fe phase (which is paramagnetic at room temperature).

1. Introduction

It has been shown that a metastable fcc FeCu phase can be formed by mechanical alloying. After subsequent annealing a precipitation of bcc iron nanocrystals in the Cu rich fcc matrix has been observed by X-ray diffraction techniques [1]. Magnetic properties of solid solutions of Fe–Cu formed by sputtering have been studied previously [2,3].

The work by Yavari et al. [1] shows an equality of the magnetic moment at room temperature for both the as-milled sample and that annealed at 950 K. By considering the difference in Curie temperatures corresponding to the fcc FeCu phase, 500 K, and that of α iron, 1000 K, such reported magnetic moments equality at 300 K suggested to us the existence of crossover in the magnetization curves at lower temperatures. Therefore, in order to analyze a possible leakage of iron magnetic moment at intermediate states of the fcc FeCu decomposition process, we have performed a study of the magnetization behavior at low temperature.

Correspondence to: Prof. A. Hernando, Instituto de Magnetismo Aplicado, UCM-RENFE, P.O. Box 155, Las Rozas, 28230 Madrid, Spain.

2. Experimental techniques

Samples were prepared by ball milling as described in ref. [1]. SQUID magnetometry, Mössbauer spectroscopy, DSC, EDX analysis, thermogravimetry and X-ray diffraction techniques were applied to as-milled and annealed samples at 820 K. Measurements were carried out from 5 to 300 K. As far as we know this range of temperatures has not been studied before in granular magnetic systems by mechanical alloying.

3. Results

Samples with composition $Fe_{52.1}Cu_{47.9}$ (at%), according to EDX analysis, exhibit in the as-milled state a nanocrystalline single fcc phase. The variation of the magnetization with the temperature follows a perfect $T^{3/2}$ Bloch law up to 200 K (fig. 1), with an exchange stiffness constant of 96.9 meVÅ^2. This is roughly three times smaller than that of pure Fe [4]. The hysteresis loops obtained at 20 and 300 K are shown in fig. 2. The average susceptibility does not change in the temperature range from 20 to 300 K, indicating that the fraction of nanocrystals exhibiting superparamagnetic behavior is negligible. The small hysteresis, with remanent value below 0.01 times the saturation magnetization and coercive field of 40 Oe, shows a negligible structural anisotropy. The lack of structural anisotropy might be a consequence of the disordered distributions of Fe and

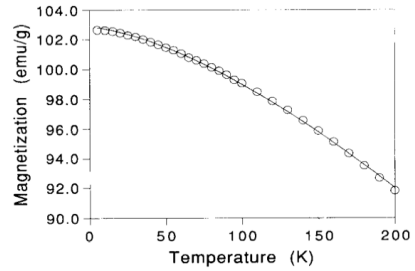

Fig. 1. Temperature dependence of the magnetization for an as-milled sample under an applied field of 5 T. The open circles are the experimental data and the solid line is the fitting according to a $T^{3/2}$ law.

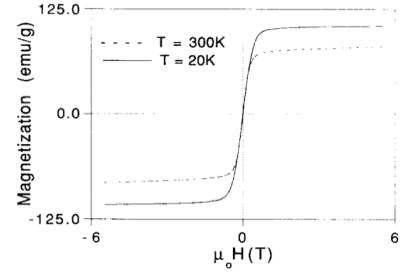

Fig. 2. Hysteresis loops corresponding to the as-milled sample at 20 and 300 K.

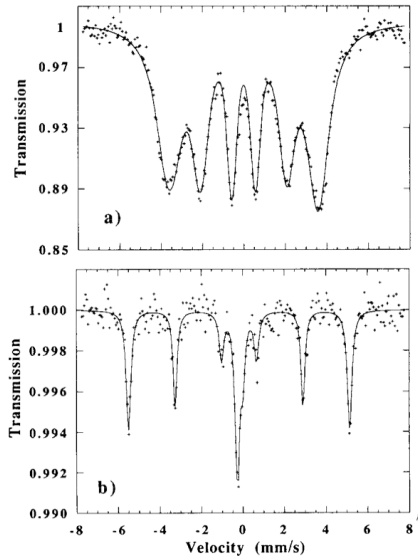

Fig. 3. Room temperature Mössbauer spectra for (a) as-milled and (b) annealed samples. The spectrum in (a) shows a broad distribution of hyperfine fields centered at 21 T and an isomer shift of +0.1 mms^{-1} relative to α-Fe at room temperature. The shoulder in the central peak in spectrum (b) shows the existence of a number of paramagnetic Fe atoms in the neighborhood of Cu atoms (see the text).

Cu atoms in the fcc structure. The Mössbauer spectrum is shown in fig. 3(a).

The as-milled sample was heated up to 820 K by DSC and its transformation monitored. The choice of the temperature and the heating rate was done on the basis of the work of Yavari [1]. 820 K lies above the peak of the exothermic reaction (which corresponds to the spinodal decomposition of the metastable solid solution) but below the total phase separation and thus we monitor an intermediate state of the Fe segregation. Thermogravimetry showed that oxidation was lower than 1% (the weight increased 0.8% during annealing). After the annealing, which causes the partial dissociation of the metastable fcc FeCu phase into Fe and Cu phases, the X-ray diffraction pattern showed the appearance of bcc Fe. Other new phases were not detected.

As shown in the curves of fig. 4 the magnetization at low temperatures is 30% smaller than the as-milled sample for the same applied field, 5 T. The Mössbauer spectrum, illustrated in fig. 3(b) and obtained at room temperature, shows a perfect pattern of crystalline bcc Fe, with a hyperfine field of 33 T, and a non-ferromagnetic phase which corresponds to 30 at% paramagnetic iron. Nevertheless, no paramagnetic behavior is observed in the low temperature M vs T curve. Furthermore, the paramagnetic peak exhibited by the Mössbauer spectrum is compatible with the corresponding γ-Fe analysis of Macedo and Keune. Here Fe atoms with a certain number of

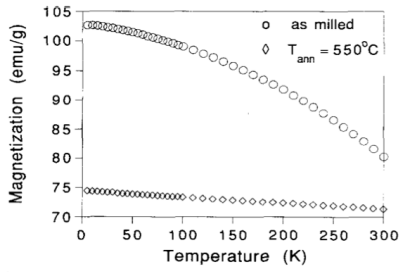

Fig. 4. Temperature dependence of the magnetization for an annealed sample under an applied field of 5 T. The curve of the as-milled sample is also shown.

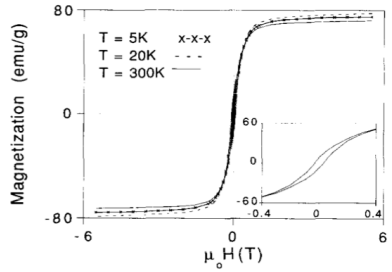

Fig. 5. Hysteresis loops for the annealed sample at 5, 20 and 300 K. The inset (in the same units) shows that the coercive field at 300 K reaches a value of 300 Oe.

Cu neighboring atoms give rise to a less intense quadrupole-splitting [5]. Since the number of Fe atoms does not change with the annealing treatment (at least not higher than 1%) and 30% behave paramagnetically at room temperature, it is reasonable to assume that these paramagnetic atoms are responsible for the 30% reduction of the saturation magnetization observed at low temperatures. However, there is no paramagnetic contribution at low temperature, and therefore we propose they are non-magnetic (with zero atomic moment) or antiferromagnetic in this low temperature range. Both observations, as well as the shape of the corresponding hysteresis loops shown in fig. 5, suggest that two types of Fe clusters have precipitated during annealing: (1) α-Fe, bcc, which is ferromagnetic and exhibits a coercive force of about 300 Oe at 300 K (fig. 5); and (2) either non-magnetic iron or γ-Fe, fcc, which is antiferromagnetic, with a transition temperature T_N ranging from 0 to 70 K according to the cluster size [6].

Since the average slope of the magnetization curve does not depend on temperature, we assume that the number of supermagnetic clusters in the range of measuring temperatures is negligible.

The absence of other crystalline phases in X-ray diffraction, the Mössbauer spectra and the reported appearance of γ-Fe in other Fe–Cu alloys obtained by sputtering or other techniques suggest the idea of a 30% γ-Fe segregation, as it

seems likely that Fe clusters with small size retain the fcc Cu phase. (We note that the lattice parameters of Cu (a = 3.616 Å) and γ-Fe (a = 3.666 Å) are similar and lead to coincidence of the X-ray diffraction peaks.)

The existence of isolated, paramagnetic or non-magnetic Fe atoms in a fcc Cu matrix can not be ruled out but it is difficult to account for 30% of the Fe atoms in this situation, as $Fe_{30}Cu_{70}$ is still a studied alloy [3] and shows no moment reduction for the Fe atoms.

4. Conclusions

The magnetic behavior of nearly equiatomic Fe–Cu alloy obtained by mechanical alloying has been studied at low temperatures for the first time. Similar magnetic measurements carried out on annealed samples have shown that the partial decomposition of the solid solution leads to a decrease of the magnetization at low temperatures. The lack of paramagnetic behavior in the low temperature range as well as the presence of a paramagnetic peak in the Mössbauer spectrum at room temperature suggest the formation of 30% γ-Fe. However, the quenching of the atomic magnetic moment of highly diluted iron atoms is a possibility which cannot be completely disregarded.

Acknowledgements

The authors are indebted to Prof. A.E. Berkowitz for helpful comments and to Dr. H.T. Savage for careful reading of the manuscript.

References

[1] A.R. Yavari, P.J. Desré and T. Benameur, Phys. Rev. Lett. 68 (1992) 2235.
[2] K. Sumiyama and Y. Nakamura, J. Magn. Magn. Mater. 35 (1983) 219.
[3] C.L. Chien, S.H. Liou, D. Kofalt, Wu Yu, T. Egami and T.R. McGuire, Phys. Rev. B 33 (1986) 3247.
[4] B.E. Argyle, S.H. Charap and E.W. Pugh, Phys. Rev. 132 (1963) 2051.
[5] W.A.A. Macedo and W. Keune, Phys. Rev. Lett. 61 (1988) 475.
[6] D.L. Williamson, W. Keune and U. Gonser, in: Proc. of the International Conference on Magnetism, Moscow 1973 (Nauka, Moscow, 1974) vol. 1, p. 246.

Materials Science Forum Vols. 235-238 (1997) pp. 559-564
online at http://www.scientific.net

CONTRAST MODULATION DURING DECOMPOSITION OF SUPERSATURATED fcc Fe-Cu SOLID AND LIQUID SOLUTIONS.

A. GARCIA ESCORIAL [1], W. BOTTA FILHO [2, 4], O. DRBOHLAV [3, 4], P. CRESPO [1, 5], M. URCHULUTEGUI [6], M. VITTORI ANTISARI [6], A. HERNANDO [5] and A. R. YAVARI [4].

[1] CENIM-CSIC, Avda. G. del Amo, 8. 28040 Madrid. Spain.
[2] Universidade Federal de Sao Carlos. Sao Carlos-SP. Brazil.
[3]Institut of Physics, CAS, Na Slovance 2, Praha 8. Czech Republic.
[4] LTPCM-CNRS, BP 75, Institut Nationale Polytechnique de Grenoble, Domaine Universitaire, St. Martin- dHerès 38402. France.
[5] I.M.A., P.O.Box 155, Las Rozas, 28230 Madrid. Spain.
[6] ENEA, CR Casaccia, Advanced Matterial Division, CP 2400, 00100 AD, Italy

Keywords: Fe-Cu solutions, spinodal decomposition

Abstract: Clear microstructural evidence is obtained from transmission electron microscopy of the occurrence of a modulated structure, as occurring in spinodal decomposition, during the decomposition of metastable mechanically alloyed $Fe_{50}Cu_{50}$ solid solutions and liquid quenched $(Fe_{20}Cu_{80})_{99}B_1$.

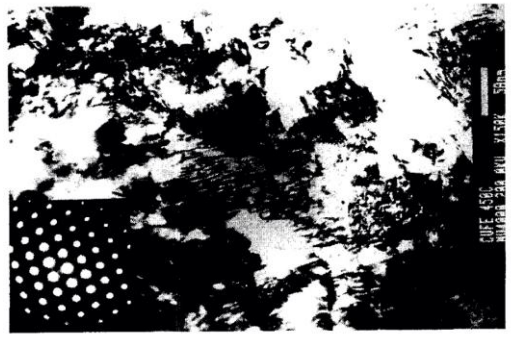

Figure 1.- TEM bright field image of $Fe_{50}Cu_{50}$ mechanically alloyed and heated up to 723 K.

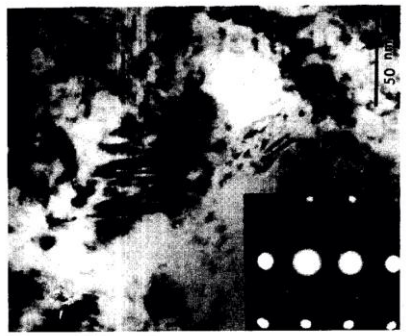

Figure 2.- TEM bright field image of $Fe_{50}Cu_{50}$ mechanically alloyed and heated up to 623 K.

Figure 3.- TEM bright field image of melt-spun $(Fe_{80}Cu_{20})_{99}B_1$.

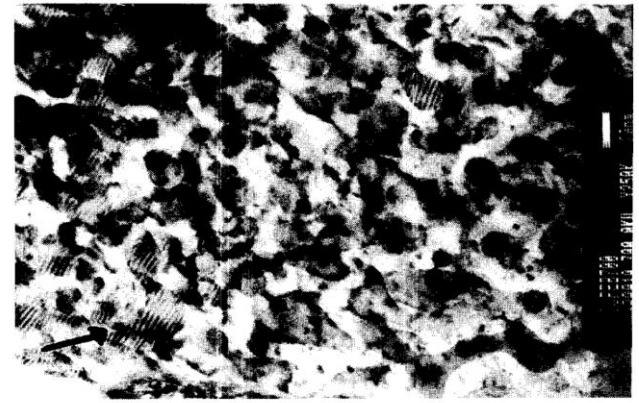

Figure 4.- TEM bright field image of melt-spun $(Fe_{80}Cu_{20})_{99}B_1$.

4. Conclusions.

In conclusion, TEM observations have shown the presence of contrast modulations in well defined crystallographic directions, with a modulating wavelength of few nanometers, which can be ascribed to spinodal decomposition in mechanically alloyed fcc $Fe_{50}Cu_{50}$ as well as of fcc $(Fe_{20}Cu_{80})_{99}B_1$ liquid solutions.

Pergamon

Acta mater. Vol. 46, No. 12, pp. 4161–4166, 1998

Printed in Great Britain
PII: S1359-6454(98)00111-6 1359-6454/98 $19.00 + 0.00

MÖSSBAUER SPECTROSCOPY EVIDENCE OF A SPINODAL MECHANISM FOR THE THERMAL DECOMPOSITION OF F.C.C. FeCu

P. CRESPO[1,2], N. MENÉNDEZ[3], J. D. TORNERO[3], M. J. BARRO[1], J. M. BARANDIARÁN[4], A. GARCÍA ESCORIAL[2]† and A. HERNANDO[1]

[1]IMA, P.O. Box 155, Las Rozas, 28230 Madrid, Spain, [2]CENIM–CSIC, Avda. G. del Amo, 8, 28040 Madrid, Spain, [3]Dpto. Química-Física Aplicada, UAM, Cantoblanco, 28049 Madrid, Spain and [4]Universidad del País Vasco, P.O. Box 644, 48080 Bilbao, Spain

In summary, low and room temperature Mössbauer spectroscopy show that the decomposition process upon thermal treatment of metastable f.c.c. FeCu solid solution gives rise to composition fluctuations, with different Fe environments. These fluctuations are evidence of the spinodal-like decomposition of the metastable FeCu solid solution.

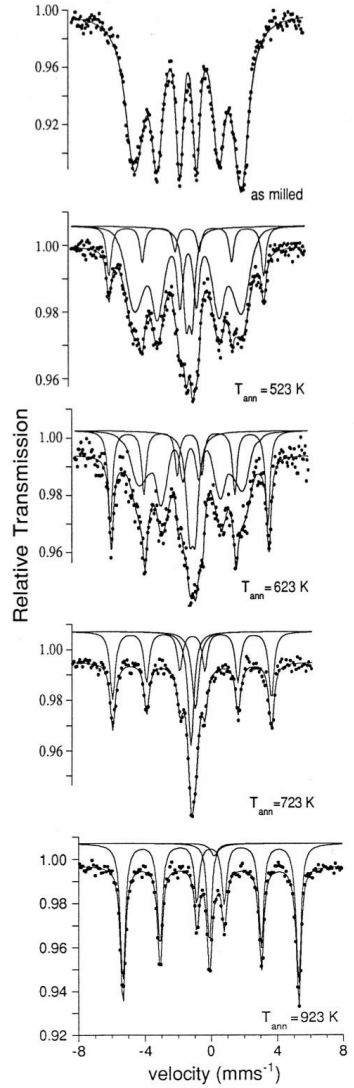

Fig. 1. Room temperature Mössbauer spectra for the as-milled and heated material.

under argon atmosphere. More details concerning the structural and magnetic characterization of the material during the heating process can be found in Ref. [5].

Mössbauer spectroscopy was performed using a ^{57}Co source embedded in a Rh matrix. The spectra were taken in a standard transmission geometry using a conventional constant acceleration spectrometer with a triangular modulation of the source. The energy calibration of the system is obtained from the spectrum of 6 μm thick α-Fe foil and all the isomer shift values are referred to the same material at room temperature. Some selected samples, the ones heated up to 723 and 923 K, were studied below room temperature between 77 and 290 K. The samples were encapsulated in a copper

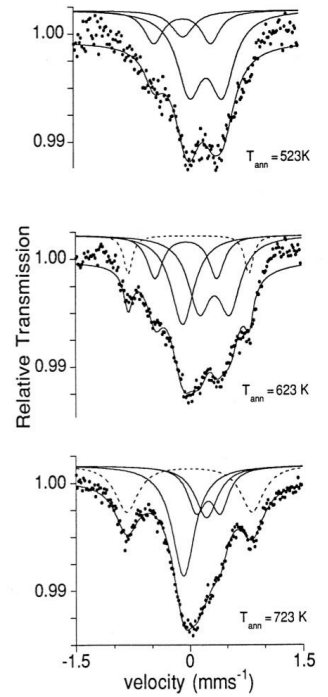

Fig. 2. Low velocity Mössbauer spectra at room temperature for the samples heated up to 523, 623 and 723 K. The dashed line corresponds to the inner lines of α-Fe. In the case of the sample heated up to 523 K, due to the low resonance absorption, these lines are not resolved in the statistics.

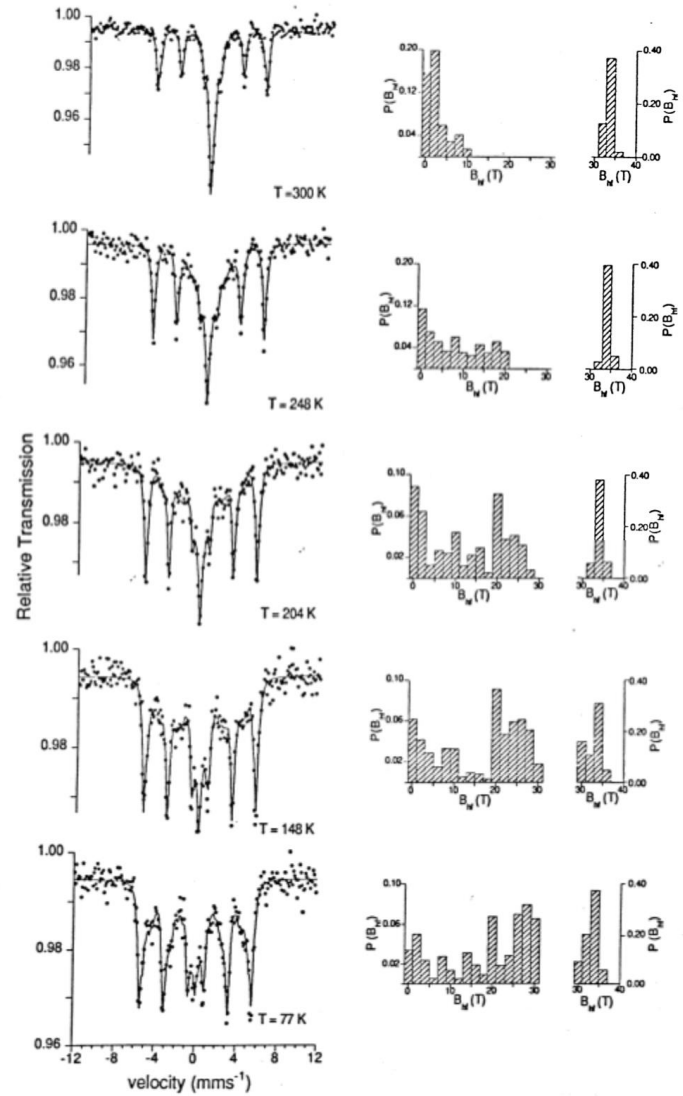

Fig. 3. Variable temperature Mössbauer spectra for the sample heated up to 723 K and the corresponding hyperfine distribution.

PHYSICAL REVIEW B VOLUME 54, NUMBER 10 1 SEPTEMBER 1996-II

Near-neighbor mixing and bond dilation in mechanically alloyed Cu-Fe

V. G. Harris, K. M. Kemner, B. N. Das, N. C. Koon, and A. E. Ehrlich
U.S. Naval Research Laboratory, Washington, D.C. 20375

J. P. Kirkland
SFA Inc., Landover, Maryland 20785

J. C. Woicik
National Institute of Standards and Technology, Gaithersburg, Maryland 20899

P. Crespo and A. Hernando
Instituto de Magnetismo Aplicado, Las Rozas, 28230 Madrid, Spain

A. Garcia Escorial
Centro Nacional de Investigaciones Metalurgicas–Centro Superior de Investigaciones Cientificas, 28040 Madrid, Spain
(Received 5 January 1996; revised manuscript received 4 April 1996)

Extended x-ray-absorption fine-structure (EXAFS) measurements were used to obtain element-specific, structural, and chemical information of the local environments around Cu and Fe atoms in high-energy ball-milled Cu_xFe_{1-x} samples ($x=0.50$ and 0.70). Analysis of the EXAFS data shows both Fe and Cu atoms reside in face-centered-cubic sites where the first coordination sphere consists of a mixture of Fe and Cu atoms in a ratio which reflects the as-prepared stoichiometry. The measured bond distances indicate a dilation in the bonds between unlike neighbors which accounts for the lattice expansion measured by x-ray diffraction. These results indicate that metastable alloys having a positive heat of mixing can be prepared via the high-energy ball-milling process. [S0163-1829(96)10033-3]

Dresden

Post-doc

Journal of Magnetism and Magnetic Materials
2 May 1996, Vol.157:61–62, doi:10.1016/0304-8853(95)01151-X
European Magnetic Materials and Applications Conference

High remanence NdFeBX (X = Cu, Si, Nb_3 Cu, Zr) powders by mechanical alloying

V. Neu, P. Crespo, R. Schäfer, J. Eckert, L. Schultz

Remanence enhancement in mechanically alloyed two-phase Nd-Fe-B magnetic material

ARTICLE *in* MATERIALS LETTERS 26(3):167-170 · FEBRUARY 1996 *with* 4 READS

IFW Dresden, Institut für Metallische Werkstoffe, Postfach, 01171 Dresden, Germany
Impact Factor: 2.49 · DOI: 10.1016/0167-577X(95)00219-7

1st Volker Neu
36.91 · Leibniz Institute for Solid State an…

2nd Uta Klement
29.04 · Chalmers University of Technology

3rd R. Schäfer

Last L. Schultz

Fe

Cu

Materials Science and Engineering: A

15 June 1997, Vol.226:577–580, doi:10.1016/S0921-5093(97)80066-4

Ninth International Conference on Rapidly Quenched and Metastable Materials

Structural and magnetic properties of nanocrystalline $(Fe\text{-}Cu)_{93}Zr_7$ alloys prepared by mechanical alloying

C. Stiller, J. Eckert, P. Crespo, S. Roth, L. Schnitz

Available online at www.sciencedirect.com
SCIENCE DIRECT®
ELSEVIER
Journal of Magnetism and Magnetic Materials 272–276 (2004) 1357–1359
Journal of magnetism and magnetic materials
www.elsevier.com/locate/jmmm

Magnetic and Mössbauer characterization of $(Fe_{0.5}Cu_{0.5})_{100-x}Zr_x$ alloys

P. Crespo[a,*], M. Multigner[a], G. Rivero[a], A. Hernando[a], A. García-Escorial[b], N. Menéndez[c], J.D. Tornero[c]

[a] *Instituto de Magnetismo Aplicado (RENFE-UCM) P.O.Box 155, 28230 Las Rozas, Madrid, Spain*
[b] *Centro Nacional de Investigaciones Metalurgicas, CSIC, Avda. Gregorio del Amo 8, 28040 Madrid, Spain*
[c] *Departamento Química Física Aplicada, UAM, 28049 Cantoblanco, Madrid, Spain*

Pd

Ferromagnetism in fcc Twinned 2.4 nm Size Pd Nanoparticles

B. Sampedro,[1,2] P. Crespo,[1,2] A. Hernando,[1,2] R. Litrán,[3] J. C. Sánchez López,[3] C. López Cartes,[3] A. Fernandez,[3] J. Ramírez,[4] J. González Calbet,[1,4] and M. Vallet[1,5]

[1]*Instituto de Magnetismo Aplicado, "Salvador Velayos," UCM, RENFE, CSIC, Las Rozas, P.O. Box 155, Madrid 28230, Spain*
[2]*Departamento de Física de Materiales, UCM, Madrid 28040, Spain*
[3]*Instituto de Ciencias de Materiales de Sevilla (ICMSE), Centro Mixto CSIC-UNIV, Sevilla 41092, Spain*

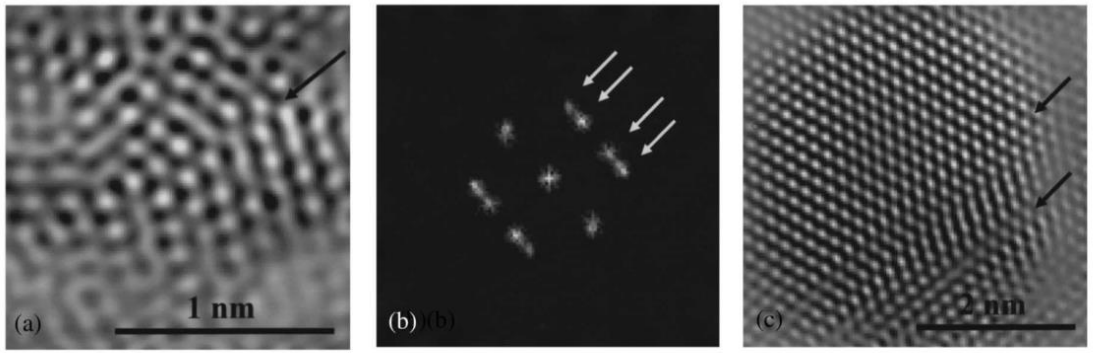

FIG. 2. (a) Fourier filtered HRTEM image of a Pd nanoparticle (diameter = 2 nm). The twin boundary is arrowed. (b) Corresponding FT diffraction pattern along the [111] direction. The splitting of the FT spots due to twinning is indicated. (c) Fourier filtered HRTEM image of a Pd nanocrystal (diameter = 4.4 nm) showing two twin boundaries.

Local deviation from cubic symmetry near the twin boundaries could also be invoked to account for the ferromagnetic behavior [5]. The strong surface energy anisotropy acts as the driving force for twinning in small Pd clusters. Therefore, the twinning boundary density is expected, and experimentally observed in this Letter and in a previous paper [6], to be noticeably enhanced in small clusters. Consequently, we suggest that the onset of ferromagnetism, experimentally observed and reported increase of $N(E_F)$ promotes the induction of a spontaneous magnetic moment.

In conclusion, we have observed the onset of ferromagnetism in fcc twinned 2.4 nm Pd nanoparticles.

saturation as is probably due to the coexistence of blocked ferromagnetic entities with superparamagnetic particles and paramagnetic atoms.

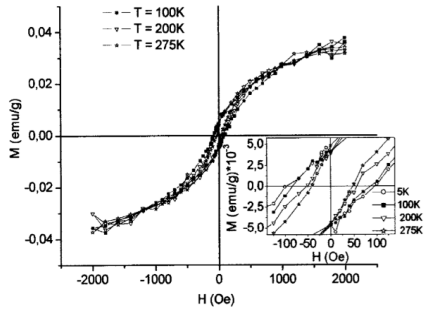

FIG. 3. Hysteresis loops at different temperatures of Pd nanoparticles. Inset: a more detailed view of the thermal coercivity response of the same sample.

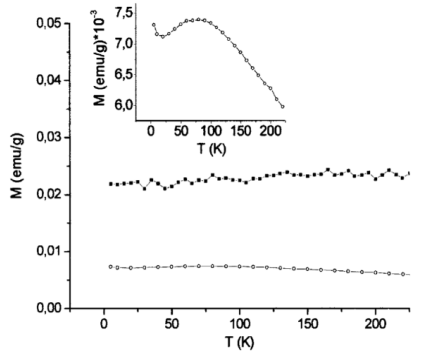

FIG. 4. Thermal dependence of magnetization under a dc applied field of 1 kOe for Pd 2.4 nm average mean particle size (solid squares) and bulk Pd (open circles). Inset: detailed thermal dependence for Pd bulk metal measured under the same applied field but plotted in a different scale.

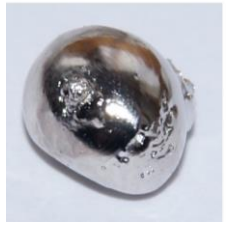

Fe + Rh

Magnetic and magnetoelastic behavior of mechanically alloyed FeRh compound

C. Marquina,[a] M. R. Ibarra, and P. A. Algarabel
Dept. Física de la Materia Condensada-ICMA, Univ. Zaragoza-CSIC, 50009 Zaragoza, Spain

A. Hernando, P. Crespo, P. Agudo, and A. R. Yavari
Instituto de Magnetismo Aplicado, Universidad Complutense, P.O. Box 155, Las Rozas, 28230 Madrid, Spain

E. Navarro
Dept. Física Aplicada I, Facultad de Veterinaria, UCM, 28040 Madrid, Spain

(Received 28 October 1996; accepted for publication 2 December 1996)

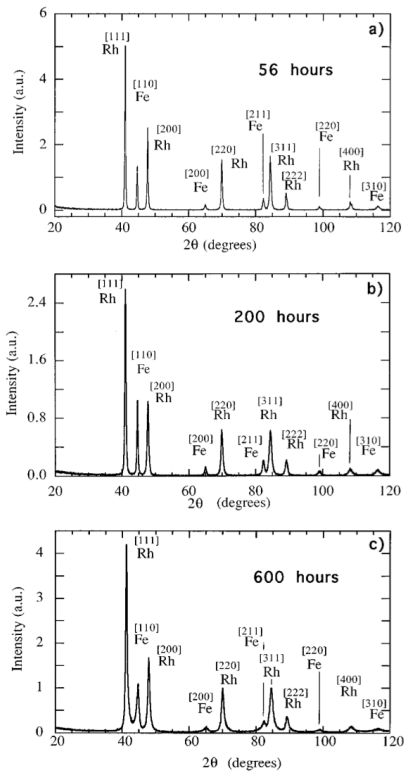

FIG. 2. X-ray diffraction patterns of the as milled sample, at different milling times, before annealing.

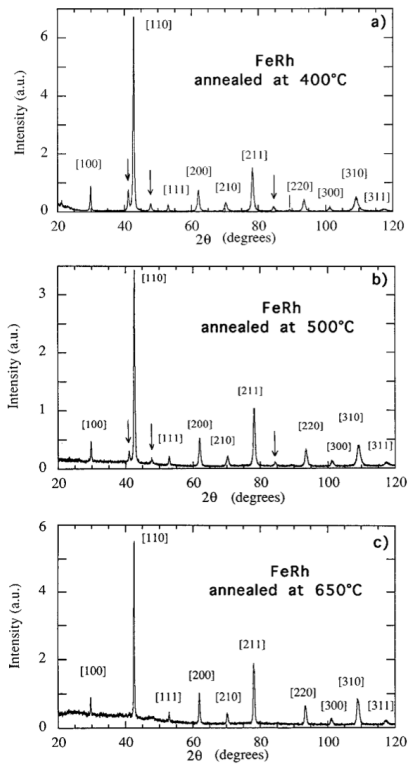

FIG. 3. Evolution of the mechanically alloyed FeRh crystal structure wi the annealing temperature (arrows indicate spurious fcc peaks).

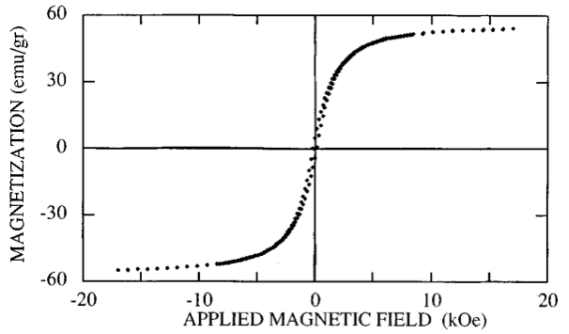

FIG. 6. Hysteresis loop of the 650 °C annealed sample, measured at room temperature.

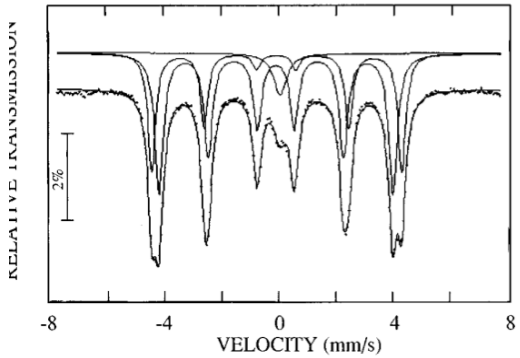

. 5. Mössbauer spectrum of the the sample annealed at 650 °C measured oom temperature.

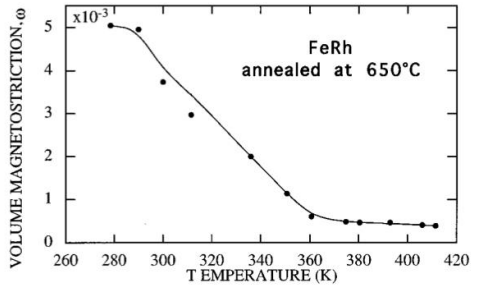

FIG. 7. Thermal dependence of the volume magnetostriction ω at 14.2 T for mechanically alloyed FeRh, annealed at 650 °C.

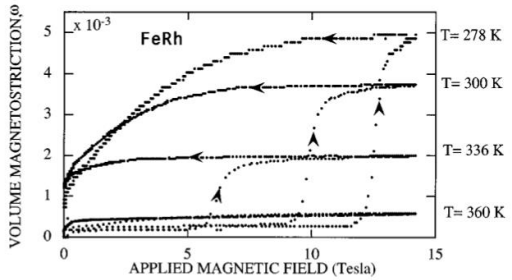

FIG. 8. Magnetostriction isotherms of mechanically alloyed FeRh, annealed at 650 °C.

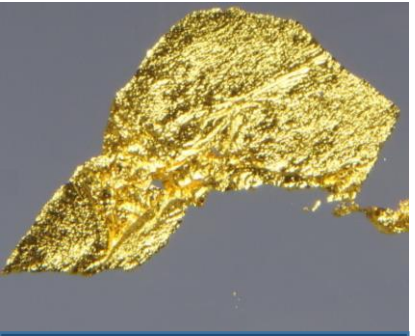

Au

VOLUME 93, NUMBER 8 PHYSICAL REVIEW LETTERS week ending 20 AUGUST 2004

350 citas

Permanent Magnetism, Magnetic Anisotropy, and Hysteresis of Thiol-Capped Gold Nanoparticles

P. Crespo,[1] R. Litrán,[2] T.C. Rojas,[2] M. Multigner,[1] J. M. de la Fuente,[3] J. C. Sánchez-López,[2] M. A. García,[1] A. Hernando,[1] S. Penadés,[3] and A. Fernández[2,*]

[1]*Instituto de Magnetismo Aplicado (RENFE-UCM-CSIC), P.O. Box 155, 28230 Las Rozas, Madrid, Spain and Departamento de Física de Materiales, Universidad Complutense, Madrid, Spain*

[2]*Instituto de Ciencia de Materiales de Sevilla CSIC-USE, Américo Vespucio nr.49, 41092 Sevilla, Spain and Departamento de Quimica Inorgánica, Universidad de Sevilla, Spain*

[3]*Grupo Carbohidratos, Laboratory of Glyconanotechnology IIQ-CSIC, Américo Vespucio nr.49, 41092 Sevilla, Spain*

(Received 13 March 2004; published 20 August 2004)

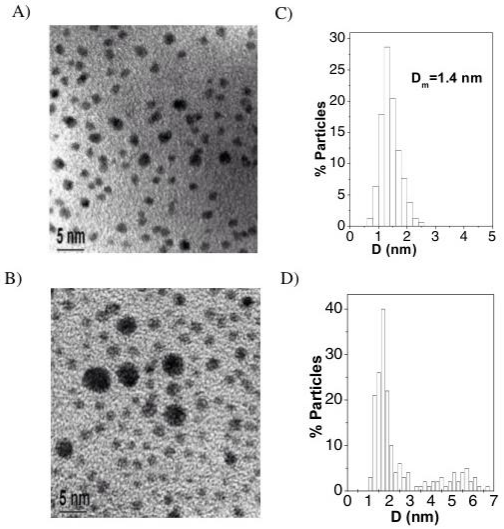

FIG. 1. Transmission electron micrographs of Au-SR (a) and Au-NR (b) NPs. Their corresponding histograms, obtained from several micrographs, are plotted, respectively, in (c) and (d).

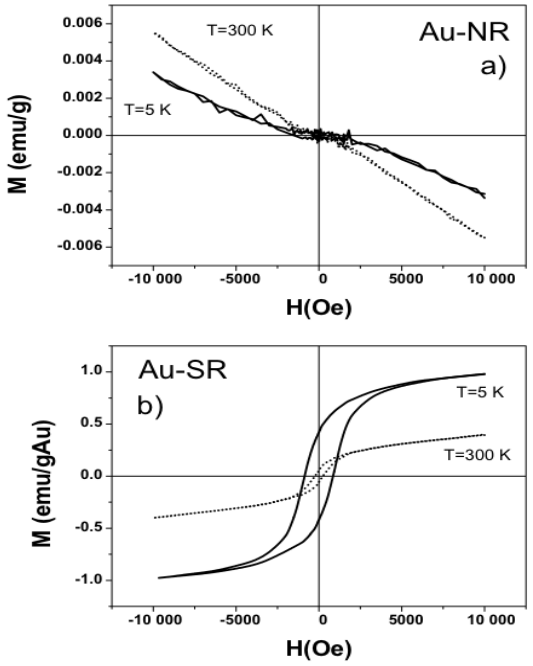

FIG. 3. Magnetization curves of gold nanoparticles stabilized by means of a surfactant, Au-NR (a), and hysteresis loops corresponding to the gold thiol-capped NPs, Au-SR (b), at 5 and 300 K. For the Au-SR sample, the magnetization is given in emu per gram of gold.

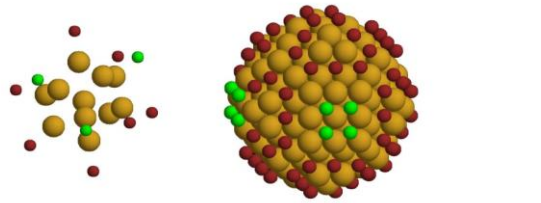

Fig. 2 Perspective view of the cluster and nanoparticle structure. On the left hand side panel, the subnanomet ric cluster Au_{11}-TPP with an icosahedral structure, whereas the fcc bulklike ~2 nm nAu-TPP nanoparticle is represented in the right hand side panel. The gold core atoms are yellow, the red balls correspond to phos phorus and the green ones to chlorine. For simplicity's sake, the aromatic rings of the triphenylphosphine molecule are not included.

UNIVERSIDAD COMPLUTENSE DE MADRID
FACULTAD DE CIENCIAS FÍSICAS
DEPARTAMENTO DE FÍSICA DE MATERIALES

TESIS DOCTORAL

Nanoestructuras multifuncionales de Fe-Au y Fe-Pt

MEMORIA PARA OPTAR AL GRADO DE DOCTOR
PRESENTADA POR

Víctor Velasco Jimeno

Directora

Patricia Crespo del Arco

Madrid, 2015

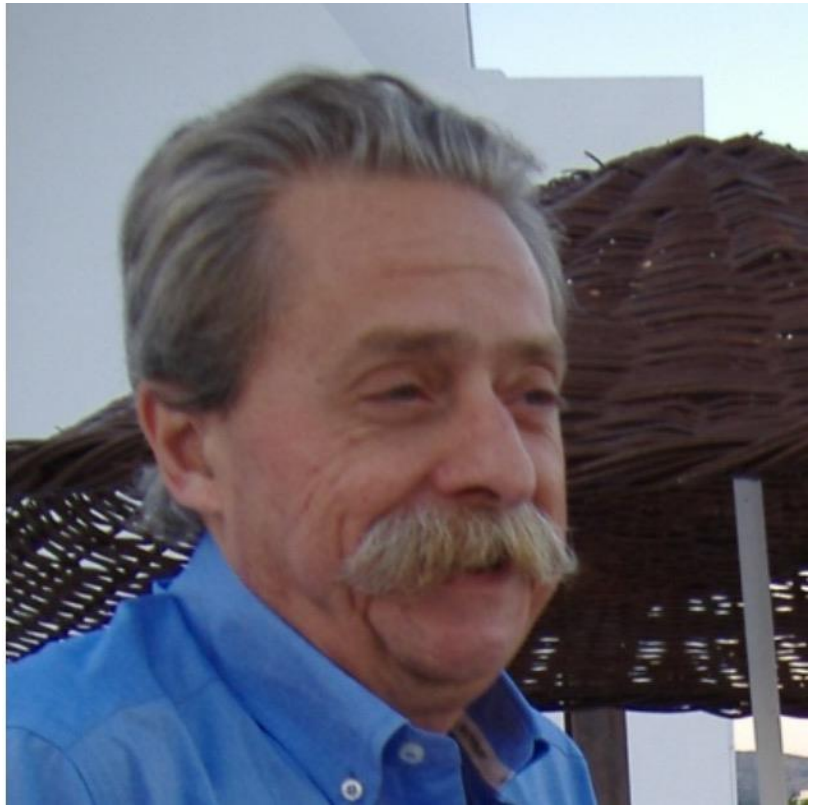

Aplicaciones

SENSORES

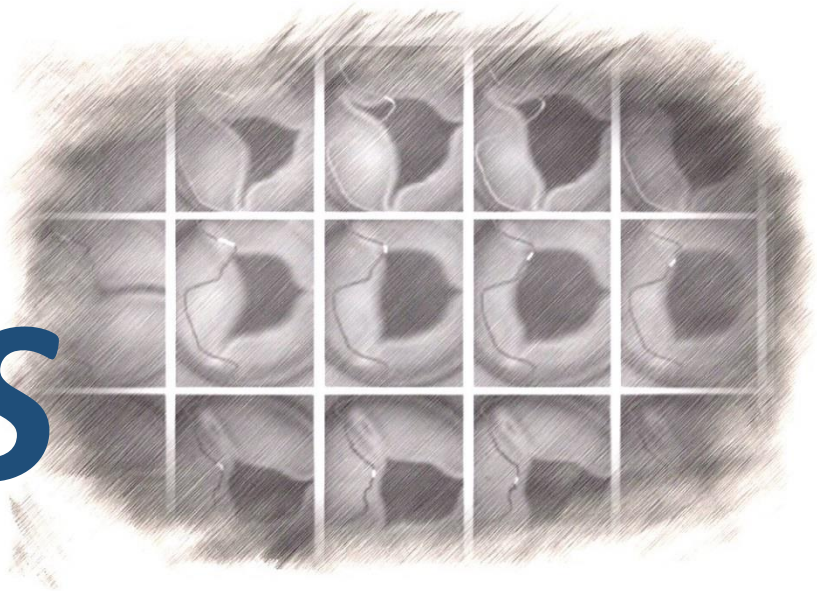

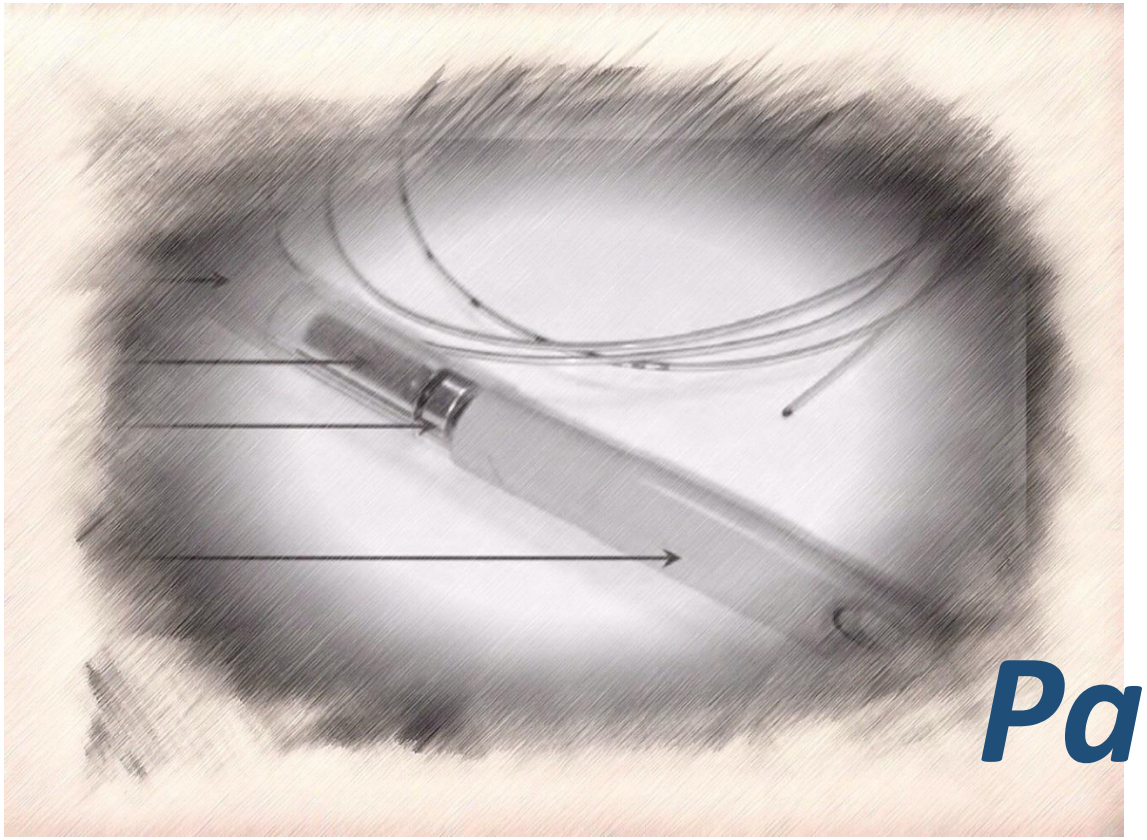

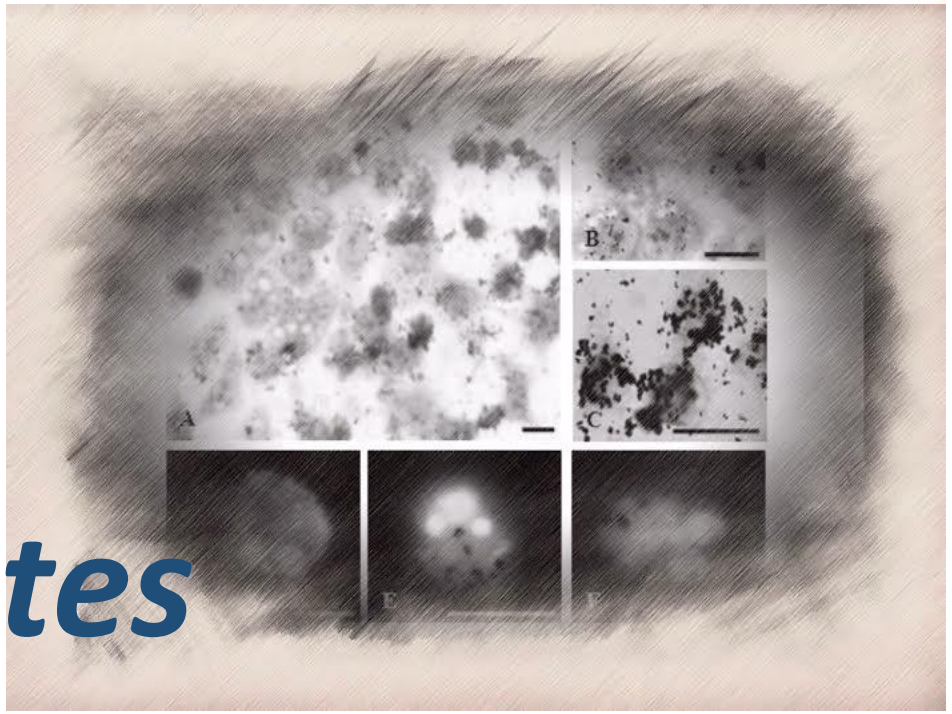

Patentes

200 años de patentes

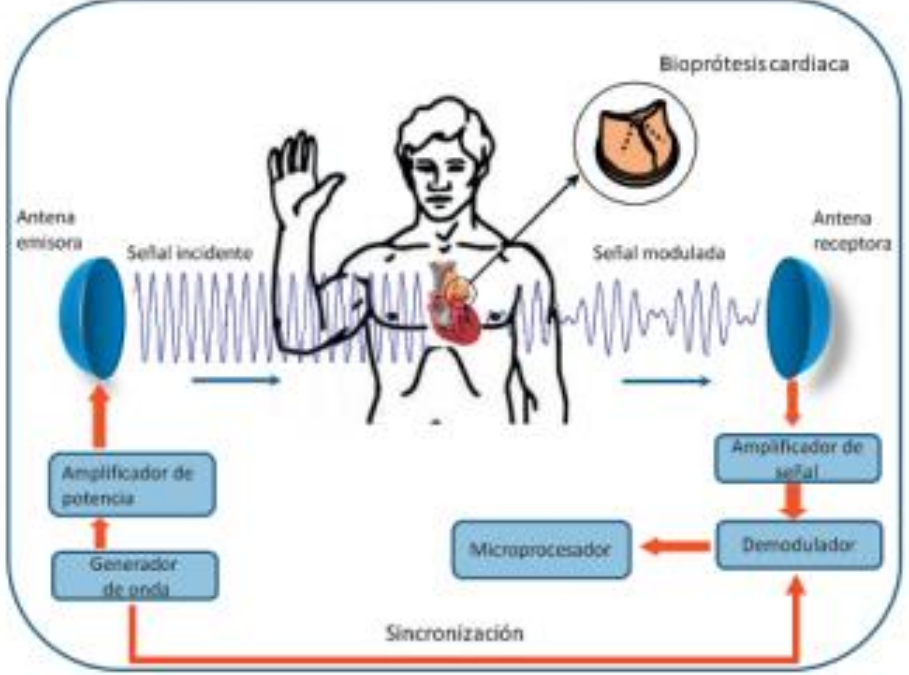

Galería 9

El Futuro de la Propiedad Industrial

El ingenio del ser humano parece no tener límites. Los nuevos avances, entre otros, en biotecnología, robótica, nuevos materiales, comunicaciones o tecnologías de la información afectarán a aspectos fundamentales de nuestras vidas. Algunas de las patentes recientemente registradas nos ofrecen claves sobre EL FUTURO DE LA PROPIEDAD INDUSTRIAL.

Tecnología médica

Las válvulas cardiacas biológicas, que a diferencia de las mecánicas no requieren mantenimiento ni tratamiento de anticoagulación, presentan sin embargo el inconveniente de una menor durabilidad y una mayor incertidumbre en su vida operativa. La invención patentada (ES 2312256) consiste en un sensor magnético que permite monitorizar el funcionamiento de estas prótesis cardiacas biológicas tras su implantación en pacientes. La utilización de este sensor evita riesgos al enfermo, ya que permite establecer con precisión el momento adecuado para la sustitución de la bioprótesis.

La invención, patentada por un grupo de investigación de la Universidad Complutense de Madrid en 2006, se basa en la incorporación de un material magnético en cada uno de los velos valvulares de la prótesis. Durante la monitorización, se hace incidir sobre la bioprótesis una onda electromagnética a una frecuencia determinada. La onda incidente es absorbida en parte por el material magnético de los velos y transmitida hacia un receptor externo al paciente. El movimiento de los velos modula la señal transmitida. Las disfunciones producidas durante el proceso de apertura y cierre de la válvula de prótesis cardiaca provocan un cambio en la señal de funcionamiento óptimo, lo que permitiría a los servicios médicos establecer con precisión el momento en el que la válvula debe ser sustituida.

En el dibujo puede verse un esquema de funcionamiento del sensor.

Imagen por gentileza de la Universidad Complutense de Madrid

23 patentes

Sort by [Upload date] Sort order [Descending] [Sort]

1. **DIFFERENTIAL CALORIMETER AND METHOD FOR MEASURING THE SPECIFIC ABSORPTION RATE OF MAGNETIC COLLOIDS SUBJECTED TO ELECTROMAGNETIC FIELDS**

Inventor:	Applicant:	CPC:	IPC:	Publication info:	Priority date:
RIVERO RODRÍGUEZ GUILLERMO [ES] MULTIGNER DOMÍNGUEZ MARTA [ES] (+4)	UNIV MADRID COMPLUTENSE [ES]	A61N1/40 G01K17/04 G01N25/4866	G01K17/04 G01N25/48 A61N1/40	WO2014181006 (A1) 2014-11-13	2013-05-10

2. **SISTEMA DE MEDIDA DE DEFORMACIONES DE RAILES FERROVIARIOS**

Inventor:	Applicant:	CPC:	IPC:	Publication info:	Priority date:
RIVERO RODRIGUEZ GUILLERMO [ES] VALDES TAMAMES JAVIER [ES] (+5)	ADMINISTRADOR DE INFRAESTRUCTURAS FERROVIARIAS ADIF [ES]	B61K9/10 B61L23/047 G01B5/30 (+1)	G01B5/30 G01N3/20 B61K9/10 (+1)	ES2391333 (A1) 2012-11-23 ES2391333 (B1) 2013-10-02	2010-12-27

3. **DISPOSITIVO Y PROCEDIMIENTO PARA DETERMINAR EL TIEMPO DE COAGULACION DE SANGRE BASADO EN MAGNETOELASTICIDAD.**

Inventor:	Applicant:	CPC:	IPC:	Publication info:	Priority date:
HERNANDO GRANDE ANTONIO [ES] FLORES VIDAL MARIA DE LA SIERRA [ES] (+6)	MICROMAG 2000 SL [ES]	G01N27/76 G01N33/4905	G01N27/76 G01N33/49	ES2373900 (A1) 2012-02-10 ES2373900 (B1) 2012-12-05	2010-07-06

4. **DISPOSITIVO PARA LA MEDIDA DE LA EVOLUCION DE LA MASA DE UN CULTIVO CELULAR "IN SITU" BASADO EN UN SENSOR MAGNETOELASTICO.**

Inventor:	Applicant:	CPC:	IPC:	Publication info:	Priority date:
CRESPO DEL ARCO PATRICIA PRESA MUNOZ DE TORO PATRICIA MARCEL (+7)	UNIV MADRID COMPLUTENSE [ES]	C12M1/3407 C12M41/36	C12M1/34	ES2352482 (A1) 2011-02-21 ES2352482 (B1) 2011-12-30	2008-07-01

5. **ESFINTER ARTIFICIAL INTRAURETRAL DE ACCIONAMIENTO MAGNETICO PARA PACIENTES FEMENINOS**

Inventor:	Applicant:	CPC:	IPC:	Publication info:	Priority date:
RIVERO RODRIGUEZ GUILLERMO MULTIGNER DOMINGUEZ MA MARTA (+3)	INDAS S A LAB		(IPC1-7): A61F2/48	AR041819 (A1) 2005-06-01	2003-10-22

6. **LOW-CONSUMPTION MAGNETIC-FIELD SENSOR**

Inventor:	Applicant:	CPC:	IPC:	Publication info:	Priority date:
RIVERO RODRIGUEZ GUILLERMO [ES] MARIN PALACIOS PILAR [ES] (+3)	MICROMAG 2000 SL [ES]	G01R33/02 G01R33/063 G01R33/18 (+2)	G01R33/02 H01B1/02 H01F1/153	ES2333575 (A1) 2010-02-23 ES2333575 (B1) 2010-11-26	2008-06-30

8. **SENSOR MAGNETICO DE DETECCION DEL DETERIORO DE PROTESIS CARDIACAS Y METODO DE DETECCION.**

Inventor:	Applicant:	CPC:	IPC:	Publication info:	Priority date:
RIVERO RODRIGUEZ GUILLERMO [ES] MULTIGNER DOMINGUEZ MARTA MARIA [ES] (+4)	UNIV MADRID COMPLUTENSE [ES]	A61B5/0002 A61F2/2472	A61F2/24 A61B5/024	ES2312256 (A1) 2009-02-16 ES2312256 (B1) 2009-12-22	2006-06-30

9. **External magnetic actuation valve for intraurethral artificial urinary sphincter**

Inventor:	Applicant:	CPC:	IPC:	Publication info:	Priority date:
RIVERO RODRIGUEZ GUILLERMO [ES] MULTIGNER DOMINGUEZ MARTA [ES] (+4)	UNIV MADRID COMPLUTENSE [ES]	A61F2/0018	A61F2/00 A61F2/04 (IPC1-7): A61F2/00	US6623421 (B1) 2003-09-23	1999-02-11

10. **Current system for compensating the magnetic field produced by electric traction railways**

Inventor:	Applicant:	CPC:	IPC:	Publication info:	Priority date:
HERNANDO GRANDE ANTONIO [ES] RIVERO RODRIGUEZ GUILLERMO [ES] (+2)	UNIV MADRID COMPLUTENSE [ES]	B60M1/06	B60M1/06 B61B13/00 H02G1/02 (+1)	US6492746 (B1) 2002-12-10	1999-02-04

11. **Miniature magnetic field sensor e.g. fluxgate, has small, ferromagnetic and helical magnetic core, which measures magnitude and direction of magnetic fields or continuous alternating fields of low frequency**

Inventor:	Applicant:	CPC:	IPC:	Publication info:	Priority date:
RIVERO RODRIGUEZ GUILLERMO [ES] HERNANDO GRANDE ANTONIO [ES] (+3)	UNIV MADRID COMPLUTENSE [ES]	G01R33/04	G01R33/04	ES2281253 (A1) 2007-09-16 ES2281253 (B2) 2008-03-16	2005-07-28

12. **Measuring device for direct measurement of magnetostriction volume of magnetic materials, comprises container holder with tight closing except for capillary section, where holder is filled with liquid**

Inventor:	Applicant:	CPC:	IPC:	Publication info:	Priority date:
RIVERO RODRIGUEZ GUILLERMO [ES] MULTIGNER RODRIGUEZ MARTA [ES] (+1)	UNIV MADRID COMPLUTENSE [ES]	G01R33/18	G01R33/18	ES2278482 (A1) 2007-08-01 ES2278482 (B1) 2008-06-16	2004-11-26

13. **MAGNETICALLY-ACTUATED ARTIFICIAL INTRAURETHRAL SPHINCTER FOR FEMALE PATIENTS**

Inventor:	Applicant:	CPC:	IPC:	Publication info:	Priority date:
RIVERO RODRIGUEZ GUILLERMO [ES] MULTIGNER DOMINGUEZ MARTA M [ES] (+4)	INDAS S A LAB [ES]	A61F2/0022 A61F2210/009	A61F2/48 (IPC1-7): A61F2/48	ES2214117 (A1) 2004-09-01 ES2214117 (B1) 2006-02-16	2002-10-22

Magnetic Sensors for Biomedical Applications

CHAPTER · MARCH 2012

Source: InTech

7

Magnetic Sensors for Biomedical Applications

Guillermo Rivero, Marta Multigner and Jorge Spottorno
Instituto de Magnetismo Aplicado (Universidad Complutense de Madrid)
Spain

2.1 *In situ* measurement of the mass evolution of cell culture

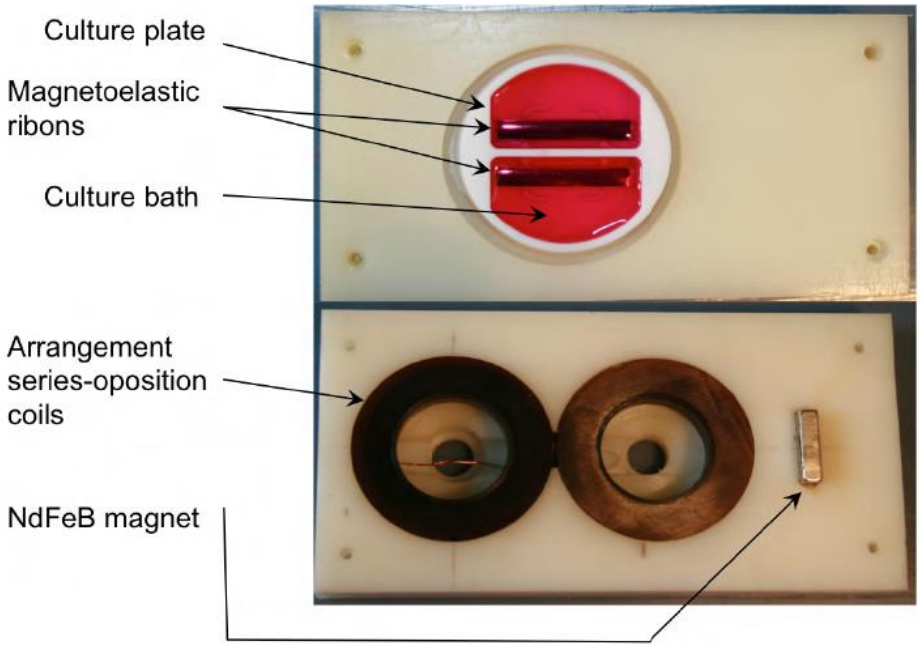

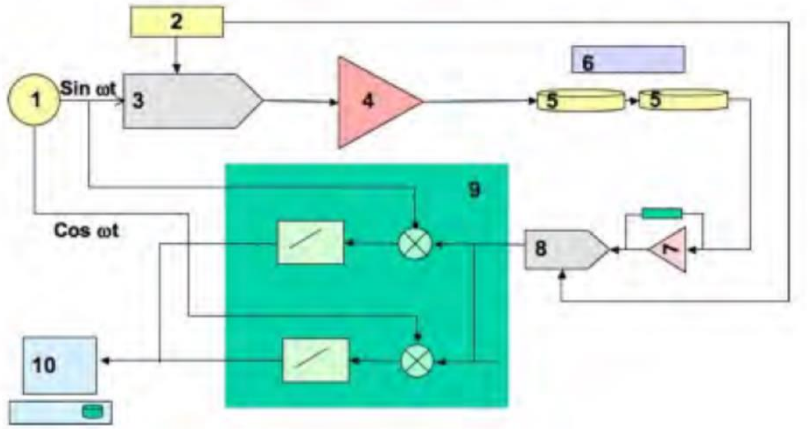

1) Direct Digital Synthesizer; 2) Voltage reference; 3) D/A Converter; 4) Power amplifier; 5) Exciting/Pick up coils; 6) Magnetoelastic sensor; 7) Voltage/Current Converter; 8) A/D converter; 9) Digital signal processor; 10) Acquisition

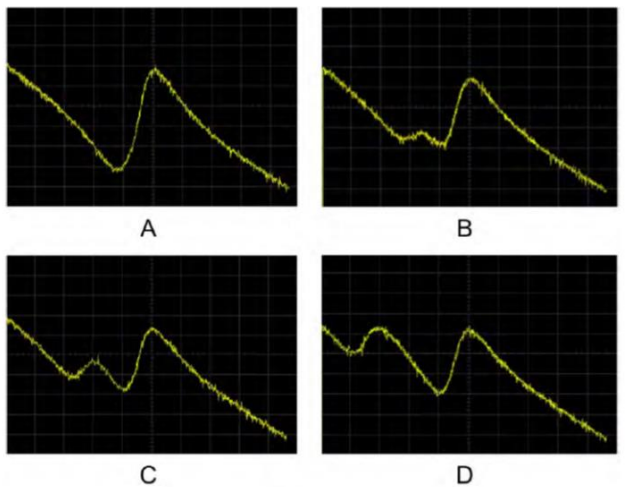

Fig. 3. Evolution of the resonance of ribbons arrangement. In the initial state A, both ribbons have the same resonance frequency. The left peak increases and decreases its frequency with the amount of mass on the corresponding ribbon.

2.2 Test of blood coagulation

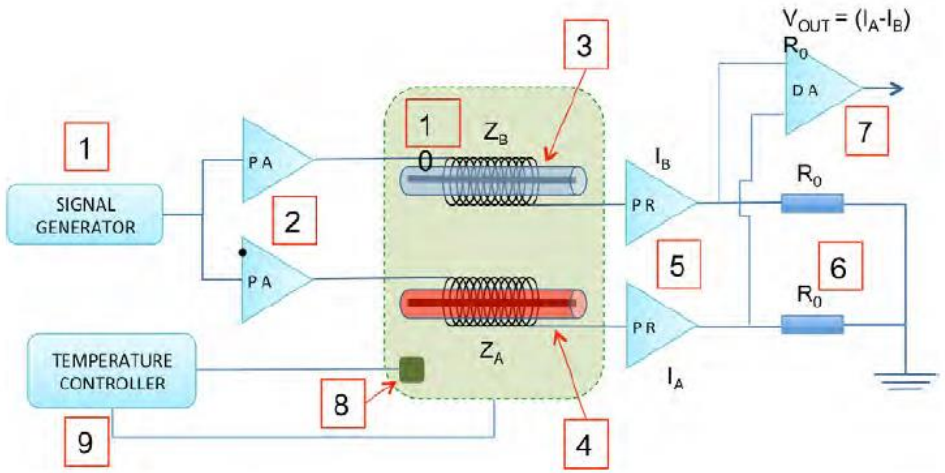

Fig. 4. Scheme of the experimental setup used to measure the blood coagulation.

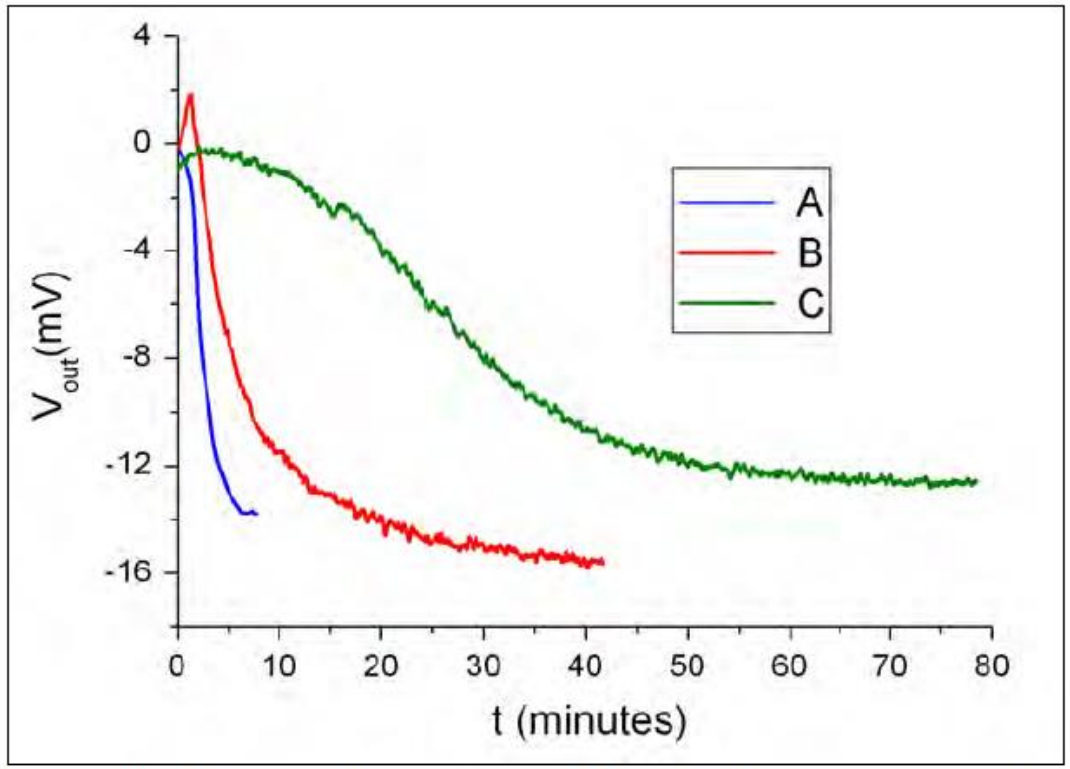

Fig. 5. Study of the influence in the coagulation of blood with different amounts of coagulant agent. The amount of blood is 200 µl, and was mixed with 5µl of coagulant (curve A), 1µl of coagulant (curve B), and without coagulant (curve C).

2.3 Sensor system for early detection of heart valve bioprostheses failure

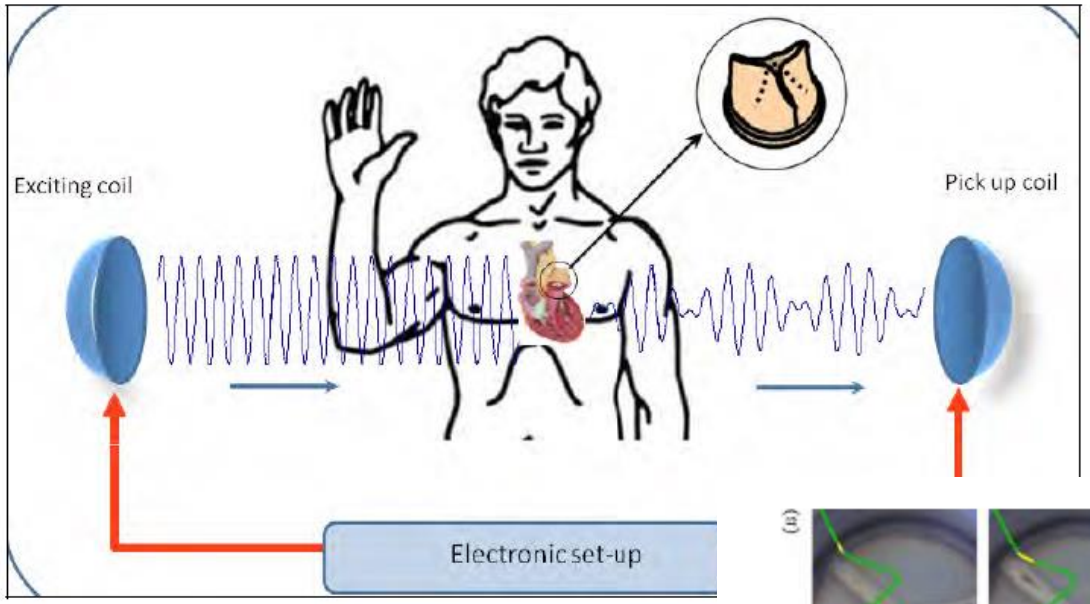

Fig. 7. Detection of motion of bioprostheses cusps with micro

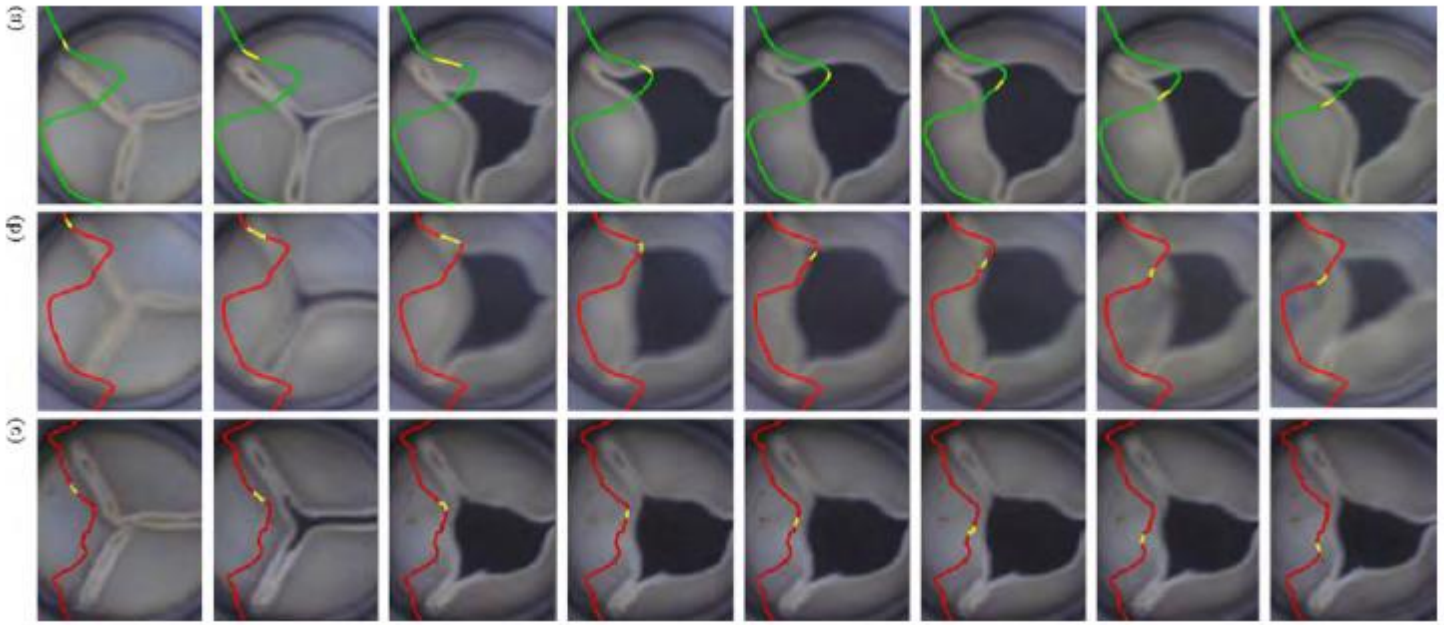

Fig. 8. Opening process of the valve with different damage levels.

3.1 Magnetic endoluminal artificial urinary sphincter

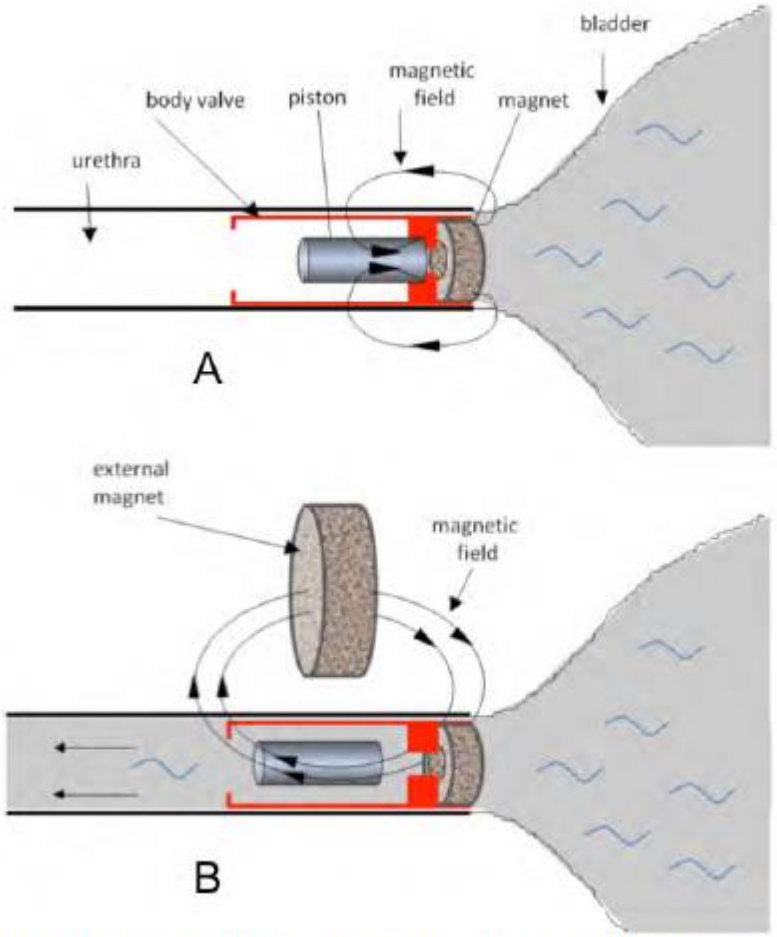

Fig. 11. Sketch of the magnetic valve operation. A) Closed position. B) Open position.

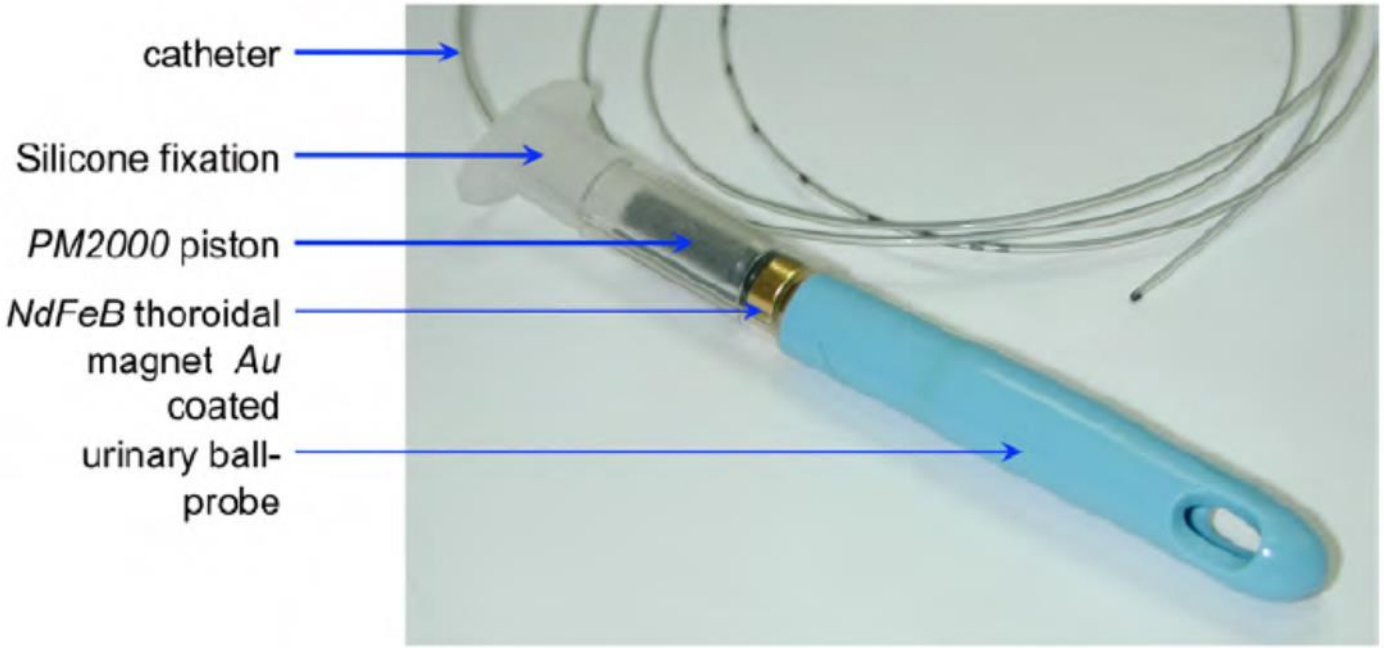

Fig. 10. Sphincter prototype for trials on animal models.

3.2 Hyperthermia HeLa cell treatment with silica-coated manganese oxide nanoparticles

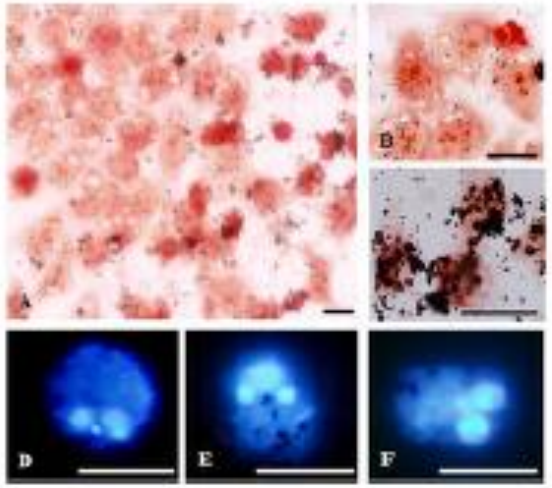

Fig. 12. Nanoparticles (black spots) inside the cell after apopthosis (White holes) (Villanueva, 2010)

THE JOURNAL OF PHYSICAL CHEMISTRY C

Article

pubs.acs.org/JPCC

Study of Heating Efficiency as a Function of Concentration, Size, and Applied Field in γ-Fe_2O_3 Nanoparticles

P. de la Presa,*[,†,‡] Y. Luengo,[§] M. Multigner,[†] R. Costo,[§,⊥] M. P. Morales,[§] G. Rivero,[†,‡] and A. Hernando[†,‡]

[†]Instituto de Magnetismo Aplicado (UCM-ADIF-CSIC), P.O. Box 155, Las Rozas, Madrid 28230, Spain

[‡]Departamento de Física de Materiales, Universidad Complutense de Madrid, Madrid, Spain

[§]Departamento de Biomateriales y Materiales Bioinspirados, Instituto de Ciencia de Materiales de Madrid/CSIC, Sor Juana Inés de la Cruz 3, Campus de Cantoblanco, Madrid 28049, Spain

[⊥]Van't Hoff Laboratory for Physical and Colloid Chemistry, Utrecht University, Padualaan 8, 3584 CH Utrecht, Netherlands

Supporting Information

ABSTRACT: The specific absorption rate (SAR) of γ-Fe_2O_3 nanoparticles (NPs) under an alternating magnetic field has been investigated as a function of size, concentration, coating, liquid carrier, and frequency and amplitude of the applied magnetic field. The NPs have been synthesized by coprecipitation method with sizes ranging from 6 to 14 nm with low polydispersity (0.2) and high crystallinity degrees. The small NPs size (6−14 nm) and the value of the maximum applied field (<7.5 kA/m) allow the use of the linear response theory for the analysis of the experimental SARs values. Under this condition, Neel−Brown relaxation times of about 10^{-7} s are obtained from SAR field frequency dependence. The NPs have been immobilized in agar to investigate the heating mechanisms, i.e., inversion of the magnetic moments inside the monodomain volume or particle rotation. The results suggest that there is a critical size of around 12 nm for obtaining the most effective heating in viscous media. Furthermore, the surface modification by aminopropylsilane coating does not affect the heating efficiency, making these NPs good candidates for hyperthermia treatment as well as model samples for standardization of hyperthermia apparatus.

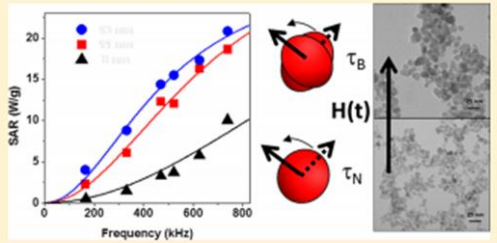

Bioelectromagnetics 33:612–619 (2012)

In Vivo Measurements of Electrical Conductivity of Porcine Organs at Low Frequency: New Method of Measurement

J. Spottorno,[1,2]* M. Multigner,[1,2] G. Rivero,[1,2] L. Álvarez,[3] J. de la Venta,[1,2] and M. Santos[3]

[1]Institute of Applied Magnetism, Madrid, Spain
[2]Department of Materials Physics, Complutense University of Madrid, Madrid, Spain
[3]University Hospital Puerta de Hierro, Madrid, Spain

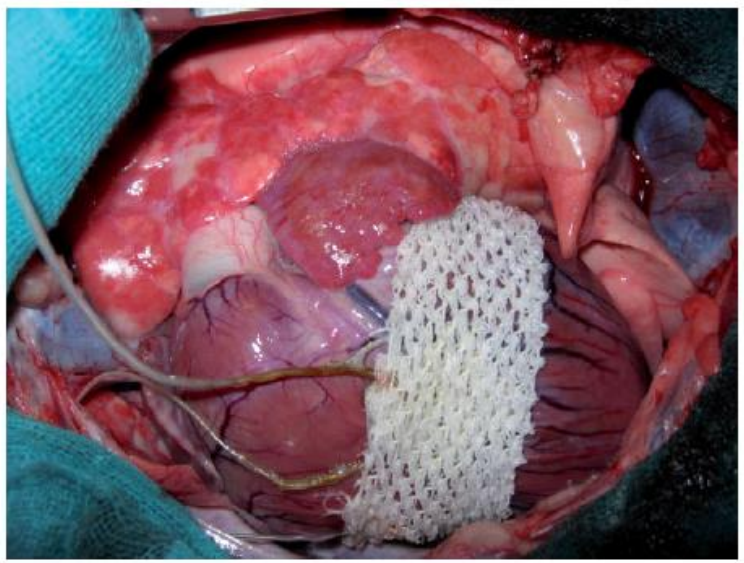

Fig. 1. Fixation of the platinum electrodes on a heart for the in vivo measurements.

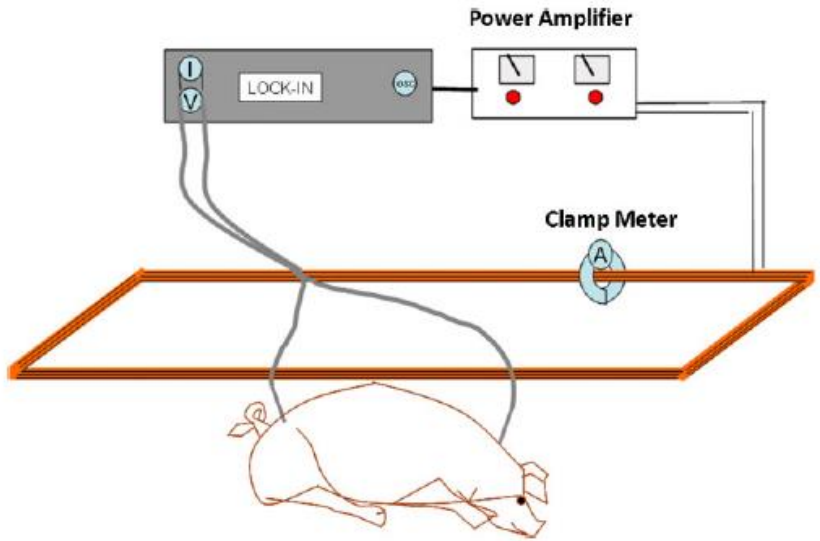

Fig. 2. Experimental setup for the in vivo measurements.

Fig. 3. Image of the measurements performed in the operating room.

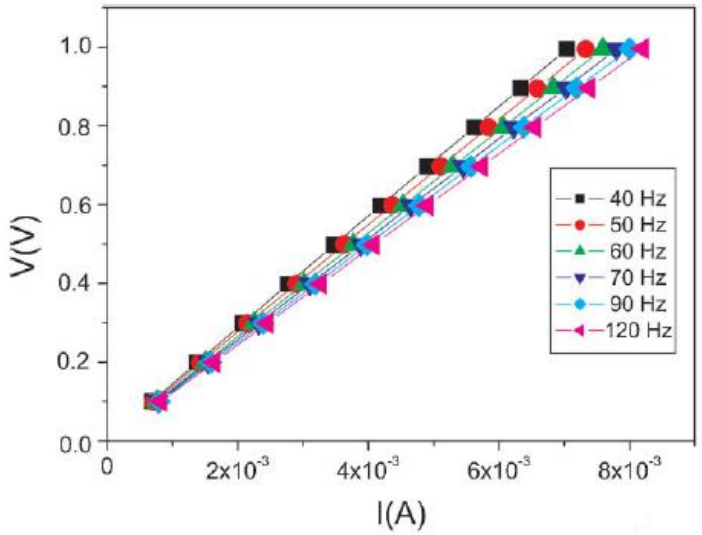

Fig. 4. Example of an I–V curve for several frequencies measured in a liver in vivo with platinum electrodes in two-electrode mode.

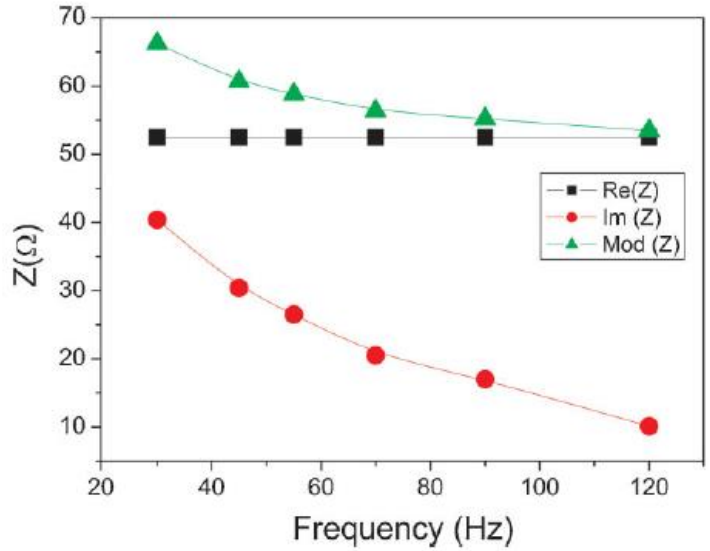

Fig. 5. Impedance of a kidney and its real and imaginary components measured with the induced voltage difference method and gold electrodes.


SIGMACAT

(19) OFICINA ESPAÑOLA DE PATENTES Y MARCAS

ESPAÑA

(11) Número de publicación: 2 391 333

(21) Número de solicitud: 201031954

(51) Int. Cl.:

G01N 3/20 (2006.01)
G01B 5/30 (2006.01)
B61K 9/10 (2006.01)
B61L 23/04 (2006.01)

(12) PATENTE DE INVENCIÓN B1

(22) Fecha de presentación:
27.12.2010

(43) Fecha de publicación de la solicitud:
23.11.2012

Fecha de la concesión:
20.09.2013

(45) Fecha de publicación de la concesión:
02.10.2013

(73) Titular/es:
ADMINISTRADOR DE INFRAESTRUCTURAS FERROVIARIAS (ADIF) (100.0%)
TITÁN Nºs 4 y 6
28045 MADRID (Madrid) ES

(72) Inventor/es:
RIVERO RODRÍGUEZ, Guillermo;
VALDÉS TAMAMES, Javier;
SPOTTORNO GINER, Jorge;
MULTIGNER DOMÍNGUEZ, Marta María;
FLORES VIDAL, María De La Sierra;
HERNANDO GRANDE, Antonio y
RODRÍGUEZ PLAZA, Miguel

(74) Agente/Representante:
UNGRÍA LÓPEZ, Javier

(54) Título: **SISTEMA DE MEDIDA DE DEFORMACIONES DE RAÍLES FERROVIARIOS**

(57) Resumen:
Sistema de medida de deformaciones de raíles ferroviarios.
Comprende uno o más sensores (1) que se fijan al raíl (3) y se caracteriza porque el sensor comprende: una célula de carga (7, 8) que genera una señal proporcional al radio de curvatura que se produce en el raíl (3) cuando se deforma por flexión; un acelerómetro de tres ejes (20) para medir las cargas dinámicas soportadas por el raíl (3) al paso del tren, que además realiza funciones de inclinómetro de dos ejes para medir la inclinación del raíl (3) tanto en sentido longitudinal como en el transversal; y un procesador de obtención de la medida de los parámetros para determinar la deformación del raíl (3). Comprende medios de comunicación inalámbrica para comunicar con otros sensores y/o con un centro de procesado y establecer la evolución de la deformación de un tramo de raíl (3).
La fijación al raíl se realiza mediante imanes (9) que facilitan su montaje/desmontaje.

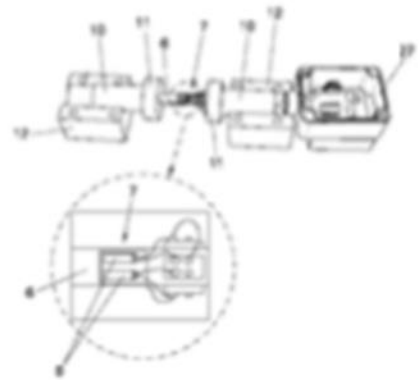

FIG. 3

ES 2 391 333 B1

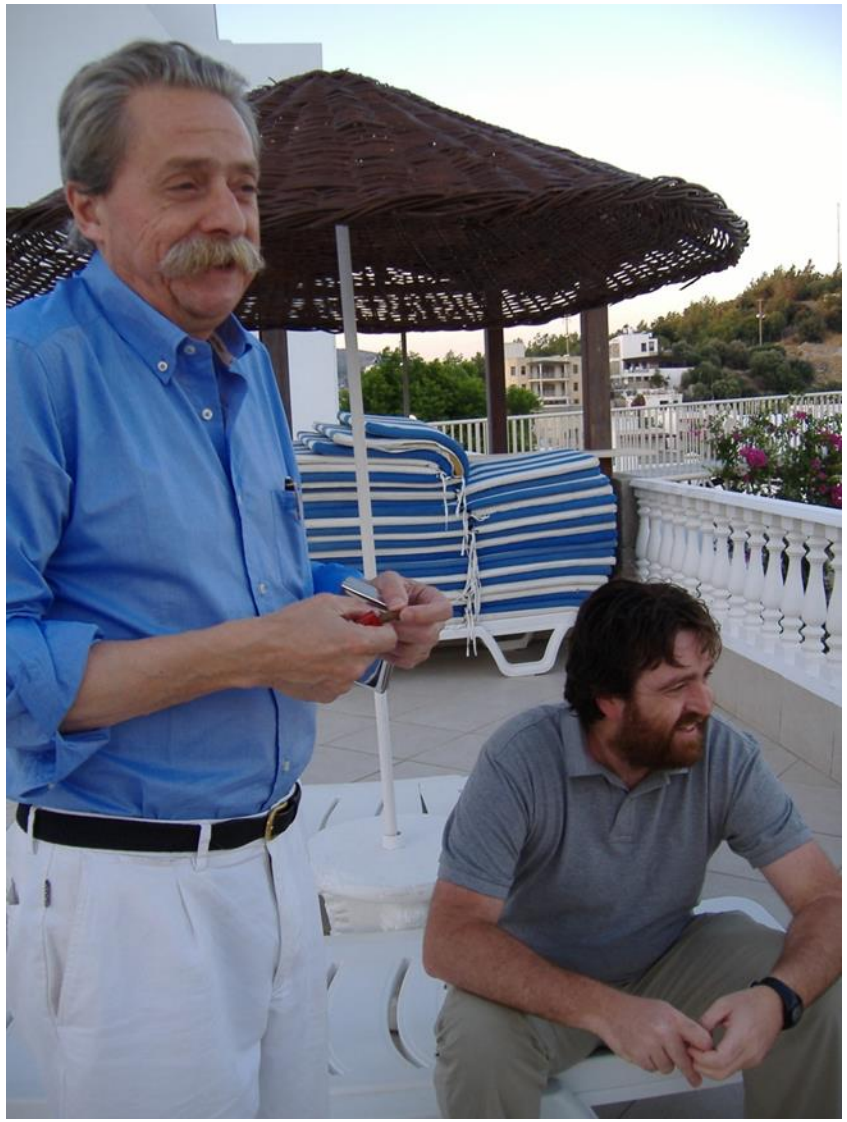

GRACIAS